

## Integrated Computational and Experimental Studies of Flapping-wing Micro Air Vehicle Aerodynamics

K Knowles  
P C Wilkins  
S A Ansari  
R W Zbikowski

Department of Aerospace, Power and Sensors  
Cranfield University  
Defence Academy of the UK  
Shrivenham, SN6 8LA, England  
[K.Knowles@cranfield.ac.uk](mailto:K.Knowles@cranfield.ac.uk)

### Abstract

This paper describes recent research on flapping-wing micro air vehicles, based on insect-like aerodynamics. A combined analytical, experimental and CFD approach is being adopted to understand and design suitable wing aerodynamics and kinematics. The CFD has used the Fluent 6 commercial code together with the grid-generating software Gambit 2; the experiments have been conducted in air and water, using various rigs and techniques. Part of our work has used 2D CFD and linear experiments (in a water tunnel). This has revealed details on vortex stability, the role of Kelvin-Helmholtz instability and Reynolds number effects. 3D CFD on rotating wings and equivalent experiments in a water tank have then been used to investigate the role of spanwise flow in the leading-edge vortex.

Key words: aerodynamics, flapping wings, low Reynolds number.

### Introduction

Agile flight inside buildings, caves and tunnels is of significant military and civilian value because current surveillance assets (such as satellites or unmanned air vehicles) possess virtually no capabilities of information-gathering inside buildings. The focus on indoor flight leads to the requirement of a distinct flight envelope. In addition, autonomy is required to enable mission-completion without the assistance of a human telepilot; this requires precise flight control. Current unmanned aerial vehicles (UAVs) are too large to achieve indoor flight and our research has concluded (see Refs [1][2][3]) that insect-like flapping flight is the optimum way to fulfil this capability — fixed wing aircraft do not have the required low-speed agility and miniature helicopters are too inefficient and noisy. Insect-like flapping flight, on the other hand, is perfectly suited for this application [4]. Insects fly at low speeds, are extremely manoeuvrable, virtually silent and most are capable of hover. In addition, insect flapping flight offers significantly better power efficiency, particularly at low flight speeds, than both fixed-wing aircraft and rotorcraft [5][6], making it ideal for our focus on micro UAVs for indoor flight.

Cranfield University at Shrivenham is engaged in world-leading research on flapping-wing micro air vehicles (FMAVs), based on insect-like aerodynamics. A micro air vehicle is defined here as a hand-sized flying machine having no dimensions greater than about 15cm. This paper will discuss how an integrated computational and experimental approach is being used in our research. The paper is organised as follows. First, the flapping-wing

Report Documentation Page				Form Approved OMB No. 0704-0188	
Public reporting burden for the collection of information is estimated to average 1 hour per response, including the time for reviewing instructions, searching existing data sources, gathering and maintaining the data needed, and completing and reviewing the collection of information. Send comments regarding this burden estimate or any other aspect of this collection of information, including suggestions for reducing this burden, to Washington Headquarters Services, Directorate for Information Operations and Reports, 1215 Jefferson Davis Highway, Suite 1204, Arlington VA 22202-4302. Respondents should be aware that notwithstanding any other provision of law, no person shall be subject to a penalty for failing to comply with a collection of information if it does not display a currently valid OMB control number.					
1. REPORT DATE <b>JUN 2007</b>		2. REPORT TYPE <b>N/A</b>		3. DATES COVERED <b>-</b>	
4. TITLE AND SUBTITLE <b>Integrated Computational and Experimental Studies of Flapping-wing Micro Air Vehicle Aerodynamics</b>				5a. CONTRACT NUMBER	
				5b. GRANT NUMBER	
				5c. PROGRAM ELEMENT NUMBER	
6. AUTHOR(S)				5d. PROJECT NUMBER	
				5e. TASK NUMBER	
				5f. WORK UNIT NUMBER	
7. PERFORMING ORGANIZATION NAME(S) AND ADDRESS(ES) <b>Department of Aerospace Engineering, University of Glasgow, UK</b>				8. PERFORMING ORGANIZATION REPORT NUMBER	
9. SPONSORING/MONITORING AGENCY NAME(S) AND ADDRESS(ES)				10. SPONSOR/MONITOR'S ACRONYM(S)	
				11. SPONSOR/MONITOR'S REPORT NUMBER(S)	
12. DISTRIBUTION/AVAILABILITY STATEMENT <b>Approved for public release, distribution unlimited</b>					
13. SUPPLEMENTARY NOTES <b>Third International Symposium on Integrating CFD and Experiments in Aerodynamics, June 2007, The original document contains color images.</b>					
14. ABSTRACT					
15. SUBJECT TERMS					
16. SECURITY CLASSIFICATION OF:			17. LIMITATION OF ABSTRACT <b>UU</b>	18. NUMBER OF PAGES <b>15</b>	19a. NAME OF RESPONSIBLE PERSON
a. REPORT <b>unclassified</b>	b. ABSTRACT <b>unclassified</b>	c. THIS PAGE <b>unclassified</b>			

problem is introduced in terms of insect wing kinematics and relevant aerodynamic phenomena. Then, a brief description of our aerodynamic model is presented, followed by descriptions of the CFD techniques used and the experiments conducted. The results of the aerodynamic modelling and the CFD are discussed, together with the available experimental data, under separate headings of 2D (or planar) flows and 3D (or rotary) flows. There is then a brief outline of how the aerodynamic model has been integrated with experimental data to address wing aeroelasticity. The paper ends with a summary of the main findings.

## Flapping-wing Problem

For the development of an engineering model to demonstrate the behaviour of insect-like flapping wings it is necessary first to understand the underlying kinematics responsible for the forces and the associated aerodynamics. Wing kinematics encompass a whole series of design parameters that can be optimised to give the desired performance, once their effects are quantified.

### Kinematics

The availability of high-speed photography has enabled reasonably good descriptions of the kinematics of insect wings [7][8][9]. The following description applies to insects with one pair of wings (diptera). The overall flapping motion is similar to the sculling motion of the oars on a rowboat, consisting essentially of three component motions — sweeping (fore and aft motion), heaving (up and down motion) and pitching (varying incidence). Flapping frequency is typically in the range 5–200 Hz. The wing motion can be divided broadly into two phases — translational and rotational. The translational phase consists of two half-strokes — the downstroke and the upstroke (see Figure 1). The downstroke refers to the motion of the wing from its rearmost position to its foremost position, relative to the body. The upstroke describes the return cycle. At either end of the half-strokes, the rotational phases come into play — stroke reversal occurs, whereby the wing rotates rapidly and reverses direction for the subsequent half-stroke. During this process, the morphological lower surface becomes the upper surface and the leading edge always leads (Figure 1a).

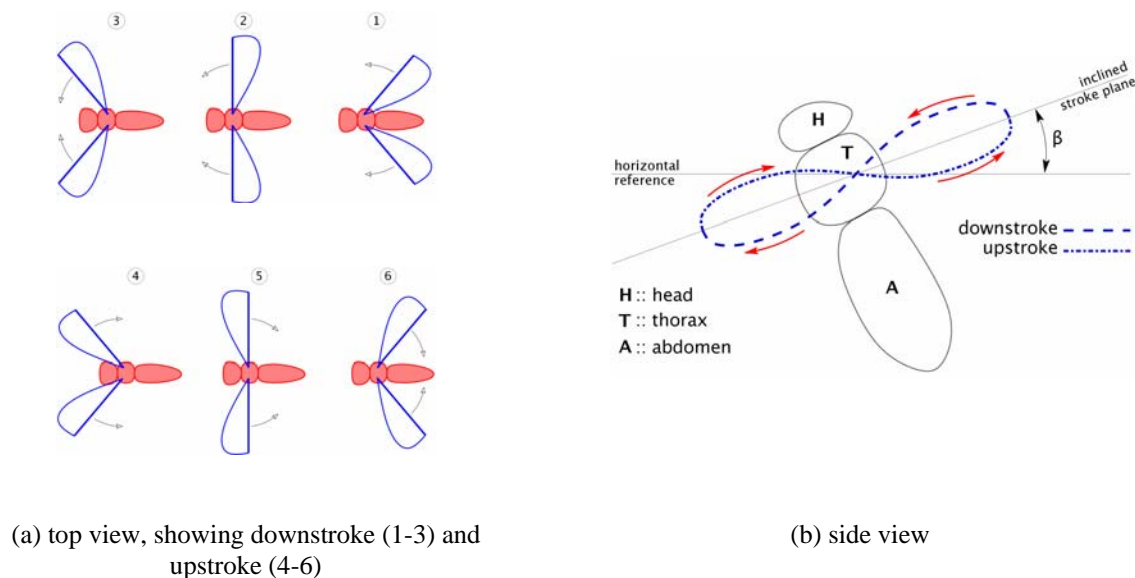


Figure 1: Insect-like flapping

The path traced out by the wing tip (relative to the body) during the wing stroke is similar to a figure-of-eight on a spherical surface (see Figure 1b) as the wing semi-span is constant. The wing flaps back and forth about a roughly constant plane called the stroke plane (analogous to the tip-path-plane for rotorcraft). The stroke plane is inclined to the horizontal at the stroke-plane angle  $\beta$  (Figure 1b). The angle swept by the wing during a half-stroke is the stroke amplitude  $\phi$ . During a half-stroke, the wing accelerates to a roughly constant speed around the middle of the half-stroke, before slowing down to rest at the end of it. The velocity during the wingbeat cycle is, therefore, non-uniform and for hover, in particular, the motion of the wing tip does not vary dramatically from a pure sinusoid [7]. Wing pitch also changes during the half-stroke, generally increasing gradually as the half-stroke proceeds. The maximum pitch angle of  $90^\circ$  will occur near the ends of each half-stroke. A maximum pitch before the wing comes to rest is referred to here as pitch advance, whereas a maximum pitch after the start of the next half-stroke is pitch delay.

### Aerodynamics

The flow associated with insect flapping flight (and scales pertaining to micro UAVs) is incompressible, laminar, unsteady and occurs at low Reynolds numbers. Despite their short stroke lengths and small Reynolds numbers, insect wings generate forces much higher than their quasi-steady equivalents due to the presence of a number of unsteady aerodynamic effects. The flow is now understood to comprise two components — attached and separated flow [10]. The attached flow refers to the freestream flow on the aerofoil as well as that due to its unsteady motion (sweeping, heaving and pitching). For insect-like flapping wings, flow separation is usually observed at both leading and trailing edges — the leading-edge vortex, which is bound to the wing for most of the duration of each half-stroke, and the trailing-edge wake, that leaves smoothly off the trailing edge. Flow is more or less attached in the remaining regions of the wing. The leading-edge vortex is believed to be responsible for the augmented forces observed [11][12].

### Aerodynamic Modelling

As part of the study of insect-like flapping flight, a nonlinear, unsteady aerodynamic model [14] has been developed to simulate this flow regime [13][15][16]; for full details see Ansari (2004)[13]. The model is inviscid and quasi-three-dimensional, and yet, shows remarkable agreement with existing experimental data, both in terms of force prediction and flowfield representation, as shown below. Consequently, it has proved to be a valuable design tool for flapping-wing problems. The simplicity of the model (due to its inviscid nature) makes it particularly useful for rapidly iterating through various wing configurations and designs, much faster than would a conventional RANS CFD model. This model has been used for parametric studies [17] - showing, amongst other things, the importance of pitch advance in controlling lift. The model also gives insight into important flow phenomena.

### Methodology

The model is quasi-three-dimensional; strip theory is used to divide the wing spanwise into chordwise sections that are each treated essentially as two-dimensional. Radial chords are used (see Figure 2) instead of straight chords because each wing section would otherwise see a significant spanwise component of incident velocity, whose effect would be un-modelled. As a result, each wing section resides in a radial cross-plane that is then unwrapped flat and the flow is solved as a planar two-dimensional problem. The overall effect on the wing is obtained by integrating along the span. The aerodynamics of flapping wings are realised using potential flow, with flow separation enforced through the Kutta-Joukowski condition at both the leading and trailing edges. The principle of linear superposition is applied — quasi-steady (wake-free) and unsteady (wake-induced) components are computed separately, and the net effect is obtained by taking their sum. The flow is solved for by satisfying the kinematic boundary conditions at the wing surface, the Kutta-Joukowski condition at the wake-inception points and by requiring that the total circulation in a control volume enclosing the system must remain constant (Kelvin's law). Conformal transformation is used and all calculations are performed in the circle plane.

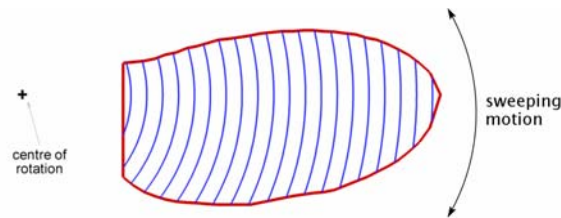


**Figure 2: Radial chords used in aerodynamic modelling**



**Figure 3: Data flow in the aerodynamic model**

### Implementation

The solution is implemented using the discrete point-vortex method. The aerofoil in each 2-D section is represented by a distribution of bound vortices and the zero through-flow condition is enforced there. The two wakes shed from the leading and trailing edges are also distributions of vorticity but these are free to move with the fluid flow. At each time-step, the quasi-steady bound circulation is computed for smooth flow at the trailing edge. Two new vortices are then released, one each from the leading and trailing edges, and placed such that they follow the trace left by the previous vortex. The nonlinear equations referred to above are then solved simultaneously for the circulation strengths of the two new vortices. At the end of the time-step, the solution is marched forward in time by convecting the shed vortices in the wake using a forward Euler scheme. During the more acute phases of the flapping cycle (e.g. stroke reversals), the time-steps are subdivided into finer sub-time-steps to give better resolution but at the cost of increased CPU time. This method gives rise to flow-visualisation which can be compared with two-dimensional experimental data (see discussion below). Forces are computed by Kelvin's method of impulses [19]. The bound and shed vortices constitute vortex pairs that impart impulses between them. The combined time-rate-of-change of impulse of all vortex pairs is a measure of the force on the wing (since only the bound vortices sustain Kutta-Joukowski forces). Moment can similarly be found from the moment of impulse.

Due to the formulation of Ansari's model (inviscid but with separation imposed at leading and trailing edges; quasi-3D using a blade element approach) a number of important fluid mechanics phenomena cannot be investigated using this approach. These include the effects of Reynolds number changes and the spanwise development of the leading-edge vortex. These will be discussed below, based on research using a complementary approach.

### CFD approach

Note that the CFD results deal only with a translating wing, not a flapping wing – it being felt more valuable to investigate this constituent part of flapping motion initially, with a view to increasing understanding of the phenomenology involved. The fluid is assumed to be incompressible (a reasonable assumption at these low Reynolds numbers) and flow is assumed to be laminar (again, due to the low Reynolds numbers).

### Software

Aerofoils and wings were drawn and meshed using the commercial grid generating software Gambit 2. Grids were then imported into the commercial CFD package Fluent 6 and the problem set up to assume incompressible, laminar flow – both reasonable assumptions at the low Reynolds numbers involved here. The second of these assumptions avoids the need to predict transition or choose a turbulence model. Motion was imposed using, in the 2D cases, velocity-inlet boundary conditions at the edges of the mesh and, in the 3D cases, a rotating reference frame. Some tests were carried out to investigate the feasibility of using a deforming or moving mesh, but the approach was found to be unsuitable.

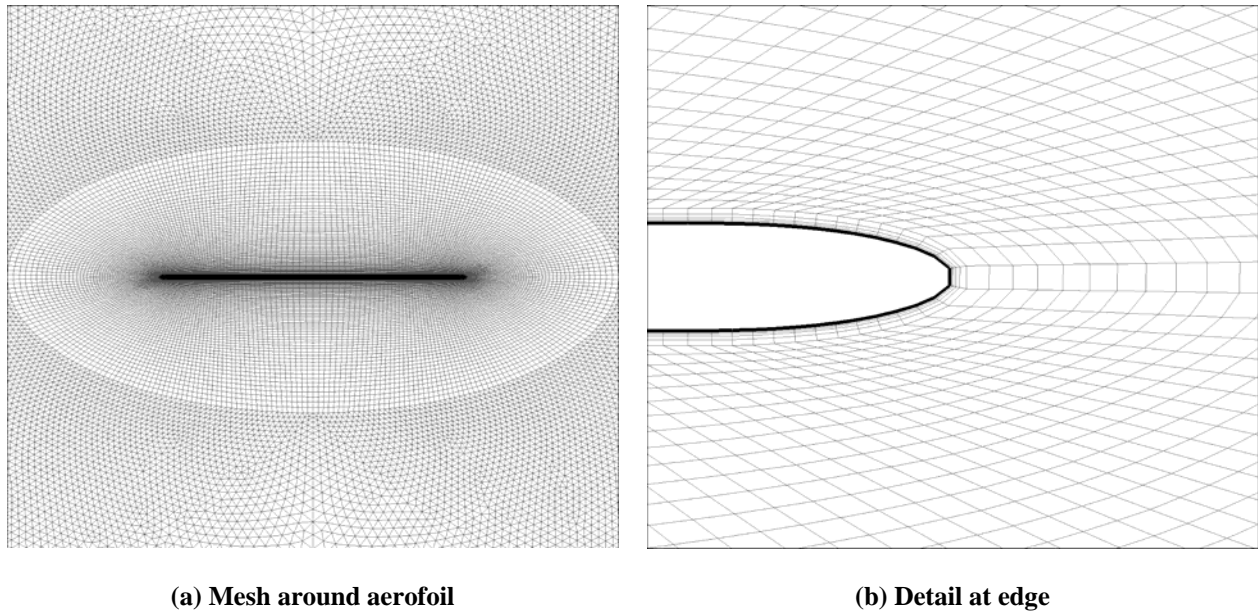


Figure 4: Mesh for aerofoil of finite thickness

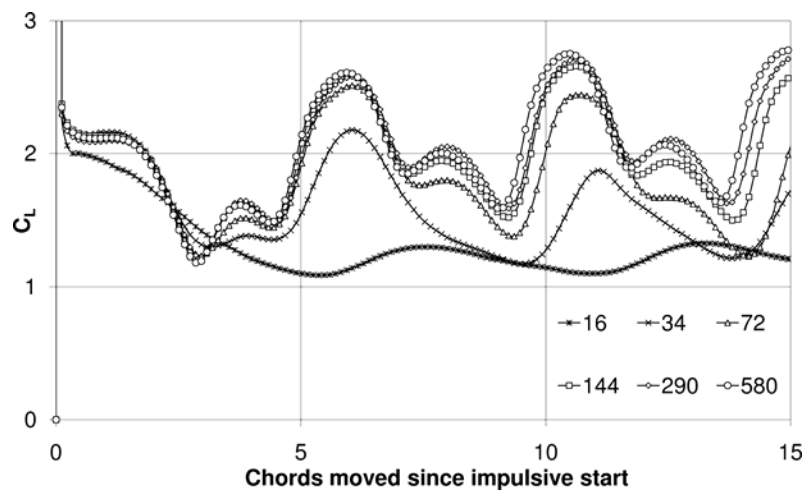


Figure 5: Mesh sensitivity. The legend numbers are the number of cells around the aerofoil's perimeter.

## Hardware

*Gambit 2* was run on a Linux workstation running *Red Hat Enterprise Linux 2.6.9* with an *Intel Pentium 4 2.80GHz* CPU and 512Mb of RAM. Some computation was also done on this machine, but most of the computation used the Shrivenham High Throughput Computer Cluster (HTCC). The HTCC consists of 17 nodes — 16 of which are used for processing and one for job submission. Each node has an identical specification — 2 x 2.2GHz Dual Core *AMD Opteron* CPUs and 16Gb of RAM per node. Most of the processing used only 4 nodes, but even for the largest 3D meshes, no simulation took longer than a week.

## Meshing

For aerofoils of finite thickness an O-grid was used close to the aerofoil with a triangular unstructured grid further from the aerofoil — see Figure 4. For infinitely thin aerofoils, an O-grid could not be used and quadrilateral cells were used close to the aerofoil, with triangular cells again being used further from the surface. In each case a boundary layer was meshed close to the aerofoil surface and mesh size was reduced close to the leading and trailing edges in order to accurately capture the separation point. The boundary was never closer than 19 chords from any point on the aerofoil. 3D simulations have used an extruded 2D mesh for simplicity. For example, to create a rectangular planform wing, the 2D mesh for an aerofoil of infinitely thin section was extruded in the direction out of the plane of the 2D mesh. 3D meshing was done such that the grid was refined near the tip and coarser near the root. Mesh sensitivity tests were carried out using an elliptical section aerofoil at 45° angle of attack by comparing the predicted lift coefficients for different mesh densities. The results are shown in Figure 5. As can be seen, refining the mesh beyond a certain value made little difference to the predicted forces. It was therefore possible to proceed with some confidence that the model was capturing all the relevant phenomena.

## Experimental methods

### Planar experiments

The main aim of the planar, or quasi-2D, experiments conducted here has been to validate the CFD model. Therefore kinematics have initially been limited to linear, constant speed (after an impulsive start) motion, and at present only flow visualisation data have been compared. It should be noted that these experiments are being referred to as “planar” (or “2D” for short) because they involve linear (rather than rotary) motions and are aimed at comparisons with (truly) 2D CFD predictions; however, the wings used are finite and will exhibit some end effects (but see below). Flow visualization was only conducted near the wing centre-section.

The planar experiments were conducted in water in order to make flow visualisation more effective. A wing was towed through a glass tank by a computer-controlled traverse, the speed being varied from run to run to change Reynolds number. The initial acceleration was very high ( $100\,000\text{ m/s}^2$ ) and final speeds were usually of the order of 0.1m/s. The wing span was such that the wing tips were very close to the sides of the tank, to minimise any spanwise effects.

In order to visualize the vortical structures around the wing, the hydrogen bubble technique has been used [22]. Although more usually used to visualize boundary layers, this method has proved simple and effective. A thin wire was attached along the leading edge of the wing, and a voltage applied between the wire and an anode placed elsewhere in the water. Hydrogen bubbles formed on the wire and were released into the flow, thus showing the leading-edge vortex. The same technique can be used to show the trailing-edge vortex sheet.

The density and size of the bubbles produced depends heavily on the diameter of the wire and the applied voltage difference. Two wires have been tested – tungsten wire of 0.01mm diameter, and stainless steel wire of 0.05mm diameter. Of these, the stainless steel wire was found to produce smaller and more uniform bubbles. An applied voltage of 12V produced good results. Increasing the voltage further tended to increase bubble size unacceptably, whereas decreasing it led to a decrease in bubble density. This technique is suitable only for a limited Reynolds number range. If Reynolds number is too low, the buoyancy of the bubbles tends to dominate their motion, leading to inaccurate results. If Reynolds number is too high, the bubbles disperse rapidly and the detailed structure of the flow becomes indiscernible. The technique was most effective at Reynolds numbers of the order of 100.

As the wire needed to be attached to the wing, it was found easiest to construct the wing from an insulating material to avoid the wing acting as a cathode. 2mm-thick glass was eventually found to be the most effective material. Although this meant that shaping the leading and trailing edges was not possible, CFD results have shown that the effect of aerofoil section is minimal as long as the aerofoil has a low thickness to chord ratio (<5%). The wing used for the results presented here has a chord of 50mm, leading to a thickness to chord ratio of 4%.

## Rotary experiments

Rotary ( or “3D”) experiments were again conducted in water. A wing was rotated around its root using a geared DC motor controlled by a variable voltage power supply. The angular velocity of rotation was variable to give Reynolds numbers (based on mean aerodynamic chord and tip velocity) from the order of 100 to the order of 10 000. At present only constant velocity rotations have been examined, i.e. angular velocity is fixed during a run.

Again, comparisons between experimental and CFD results for 3D flows have so far been limited to flow visualization. The hydrogen bubble technique was again used with the same parameters as for 2D flows. Bubbles have generally been released from the leading edge of the wing near the root to show any spanwise flow.

## Results

### 2D flows

The aerodynamic model and the 2D CFD can be compared with 2D flow visualisation experiments to validate the flowfield predictions. Agreement between all three sets of data is very good (see Figure 6).

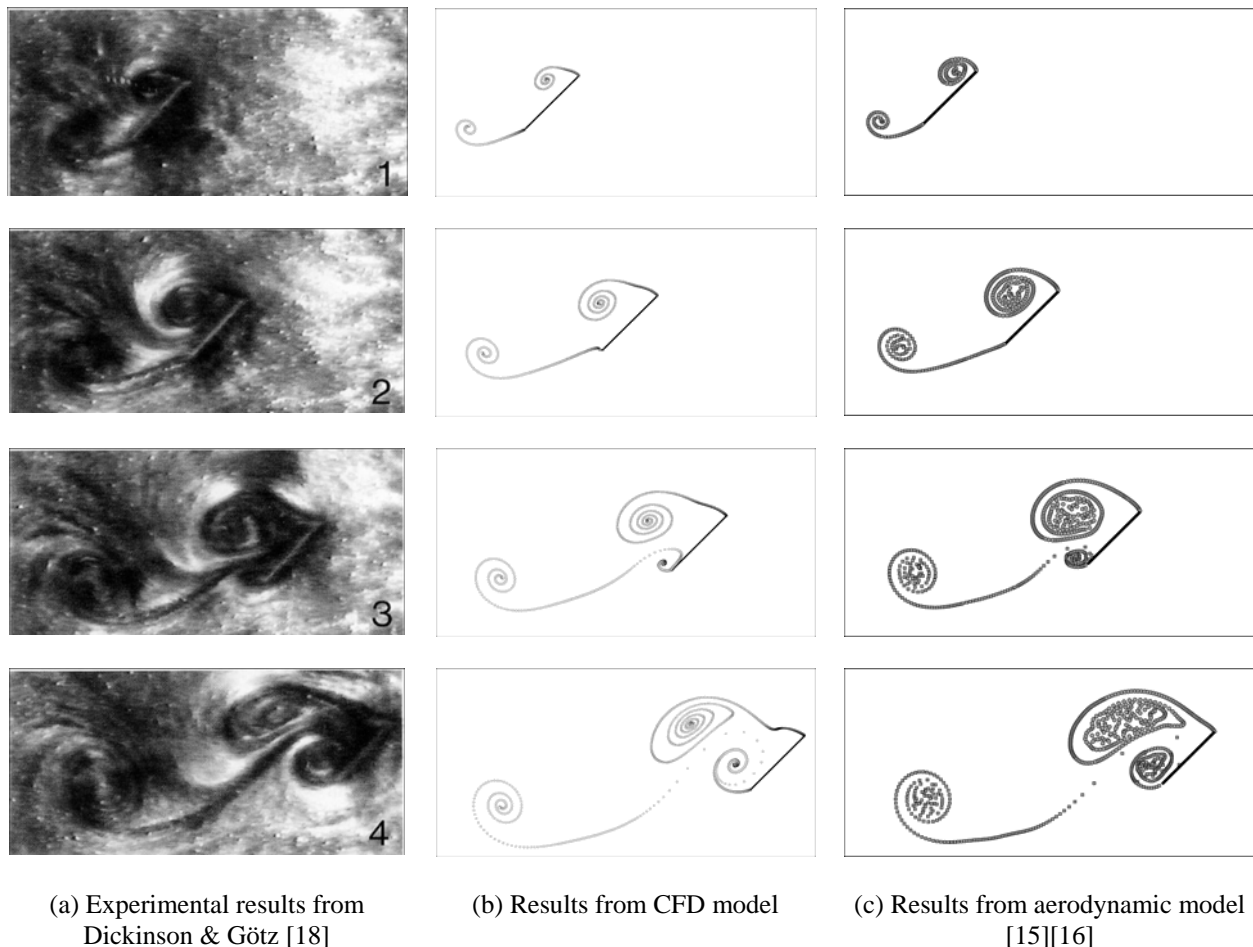


**Figure 6: Comparison of flow visualisation for flat plate aerofoil having moved (from top) 1, 2, 3 and 4 chords since being impulsively started.**

Results from the 2D experiments carried out here can also be compared to CFD results. Again, the agreement is



good (see Figure 7).

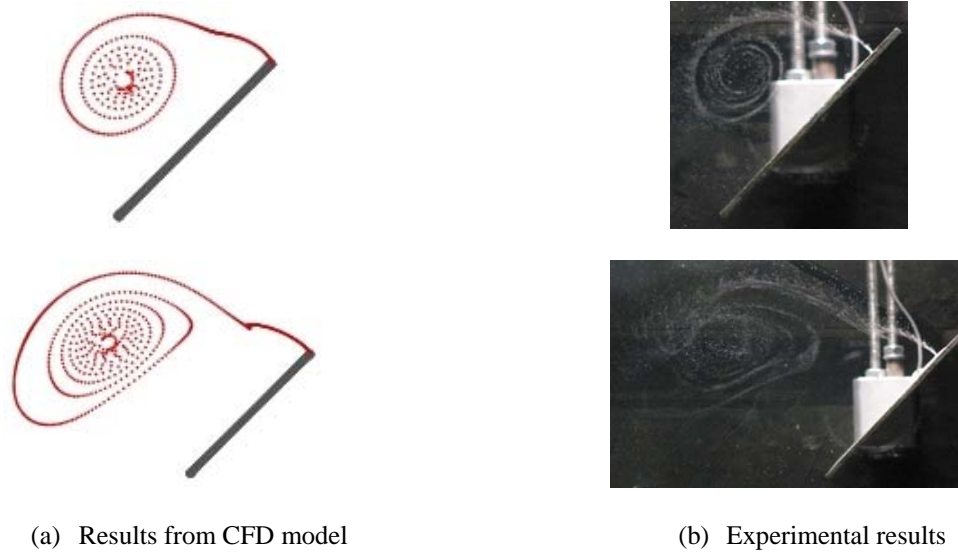


**Figure 7: Comparison of flow visualisation for flat plate aerofoil having travelled (from top) 2 and 4 chords since being impulsively started.**

Using these three approaches – experimental, CFD, and aerodynamic or analytical, the phenomenology of this type of flow can be established. As can be seen from the flow visualisation above, an aerofoil at these high angles of attack in planar motion sheds vortices alternately from leading and trailing edges. This shedding leads to periodic force fluctuations; the effect that each vortex has on the lift force is shown in Figure 8.

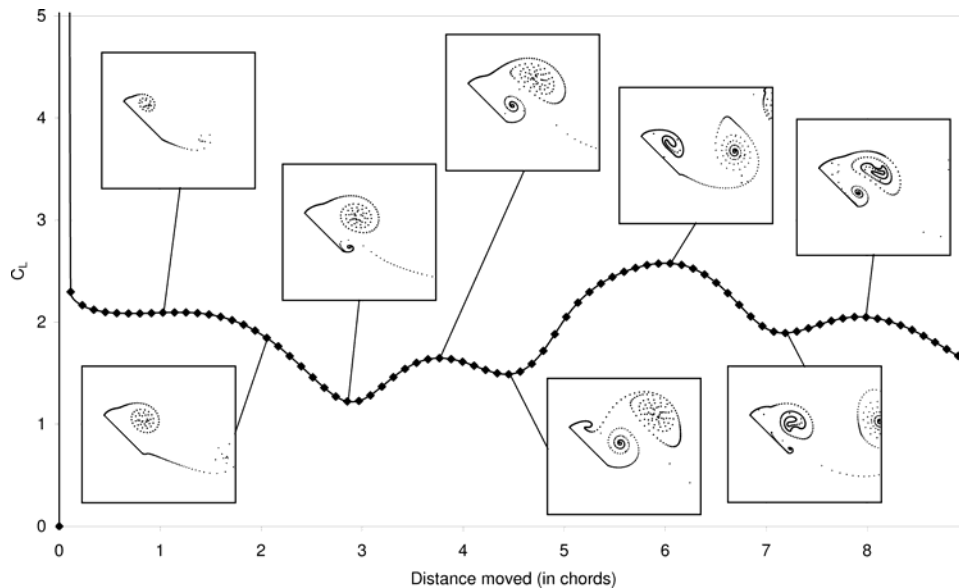


**Figure 8: Lift coefficient vs. chords moved (since an impulsive start) for a flat plate aerofoil at 45° angle of attack, showing structure of vortex shedding. Data from CFD simulation.**

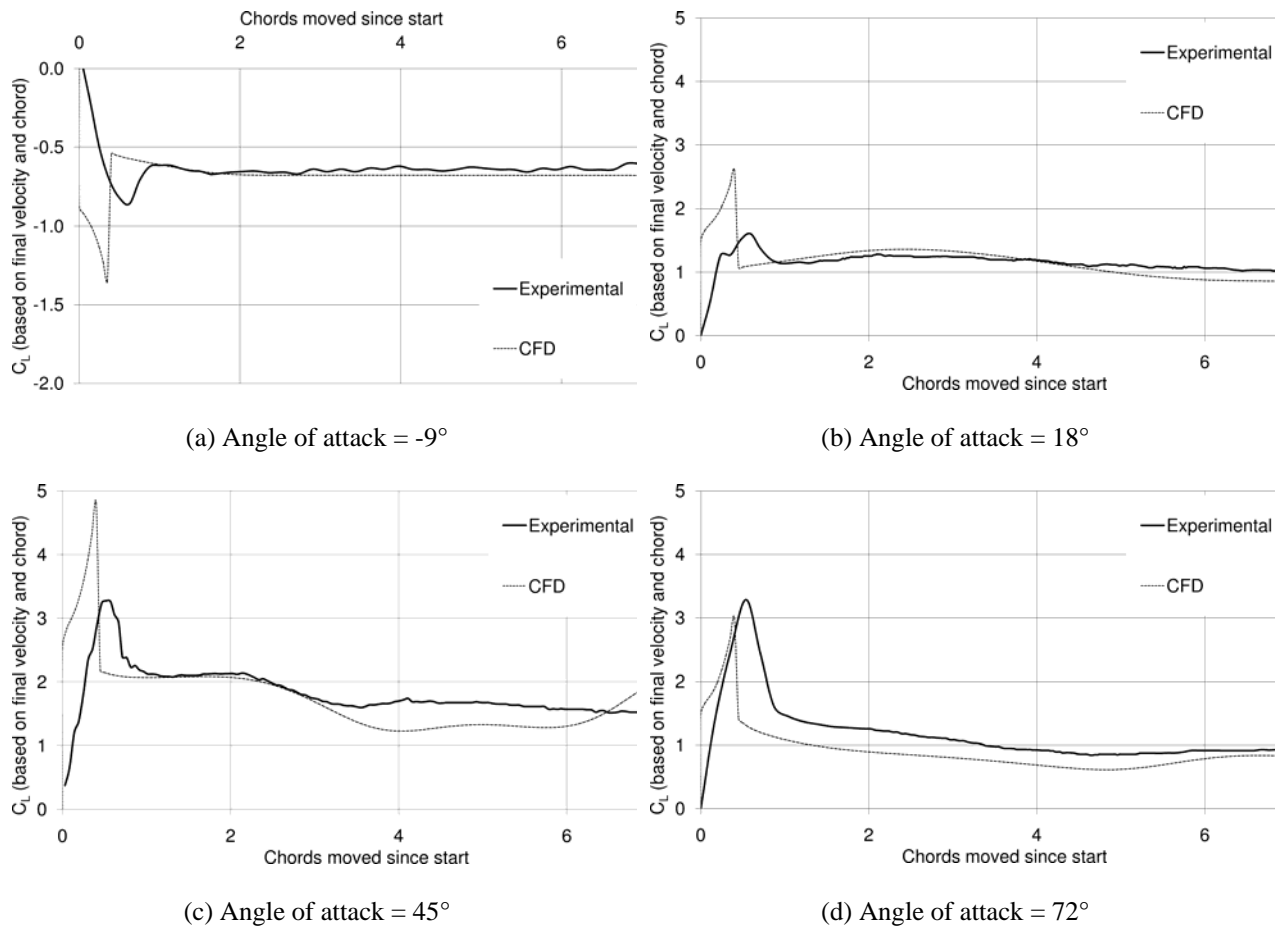


**Figure 9: Lift coefficient vs distance travelled - comparison of experimental [18] and CFD data for  $Re = 192$ .**

In addition to these comparisons of flow visualisation, we can also compare forces. Dickinson & Götz [18] measured the lift produced by their wing, and both the aerodynamic model and the CFD model can predict the lift produced by the aerofoil. Figure 9 shows comparisons between CFD and experimental results for different angles of attack. Again, the agreement is good. The discrepancy in the initial peak can be explained by considering the fact that the physical wing (and mounting hardware) used in the experiments had inertia, so would not respond instantly to instantaneous changes in lift. The non-physical CFD aerofoil had no inertia and thus any changes in lift – no matter how rapid – are captured.

Comparisons can also be made between the CFD results and the results of the aerodynamic model. However in this case we encounter a difficulty, because the aerodynamic model is inviscid and therefore Reynolds number is undefined. What Reynolds number should CFD simulations use to produce data that can be compared to the results from the aerodynamic model? In order to answer this question, Figure 10 compares data from the aerodynamic model [14] with CFD data for two Reynolds numbers. It can be seen that the low Reynolds number CFD data fails to closely match the data from the aerodynamic model. This might be expected, as the CFD model assumes a comparatively viscous fluid. When the CFD model assumes a less viscous fluid (i.e. in the higher Reynolds number case) the agreement is much better, although some high frequency fluctuations are now seen that are not shown by the aerodynamic model.

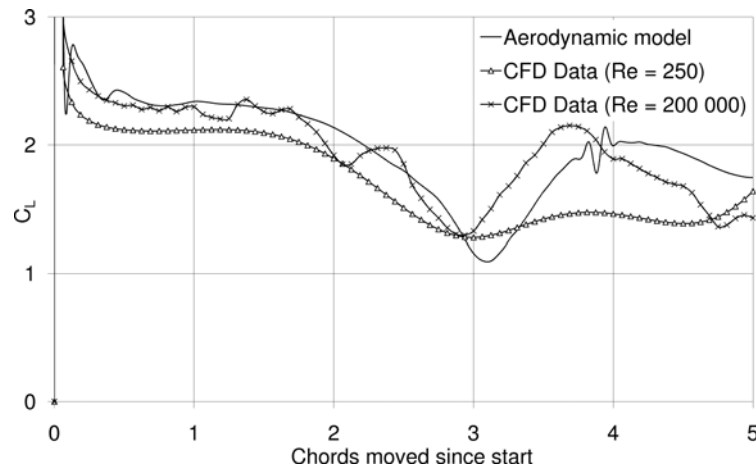


**Figure 10: Comparison of lift coefficient vs distance travelled for aerodynamic model and CFD data for two Reynolds numbers. Angle of attack = 45°.**

Examination of the CFD data reveals the reason for these fluctuations. It is seen that at Reynolds numbers above 1000 the vortex sheets tend to break down. This breakdown leads to small, relatively high frequency fluctuations in lift. The aerodynamic model does not capture this breakdown as it is the result of a viscous phenomenon. This breakdown – which is due to Kelvin-Helmholtz instability [23]**Error! Reference source not found.** – is shown in Figure 11, where for  $Re = 500$  the leading- and trailing-edge vortex sheets remain smooth and unbroken. For  $Re = 5000$ , however, the sheets break down and the vortices become less coherent. This breakdown does not affect the frequency at which the main leading- and trailing-edge vortices are shed.

### 3D flows with rotary motion

The aerodynamic model is designed to analyse insect-like flapping, where the wings move through only a small sweep angle before reversing. Therefore it may be of interest to examine how results from it compare to the results from 3D CFD simulations for cases where the wing is swept continually rather than flapped. We might expect large differences, because the aerodynamic model is quasi-2D in nature (using a blade-element approach but with rotary motion correctly represented) and therefore cannot incorporate spanwise flow effects, which are thought to be vital in stabilising the LEV.

3D CFD results reveal an LEV that is fully stable after an initial transient. During this initial transient the LEV grows until it reaches a stable size. It then remains at this size for as long as the wing continues to sweep. An example of the eventual form of the LEV is shown in Figure 12.

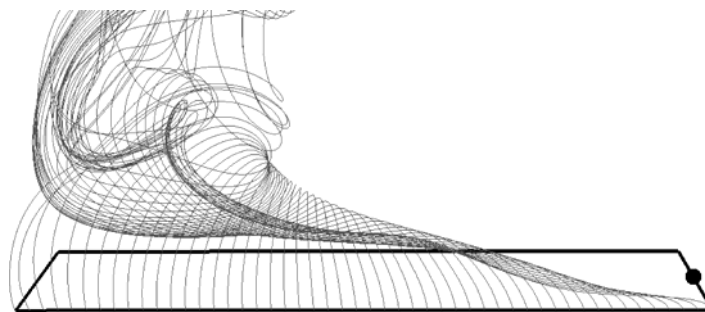


**Figure 12: 3D LEV (shown by streamlines released from leading edge) for Reynolds number of 500 (based on wing chord and tip velocity). The wing is rotating around the black circle at an angle of attack of 45°.**

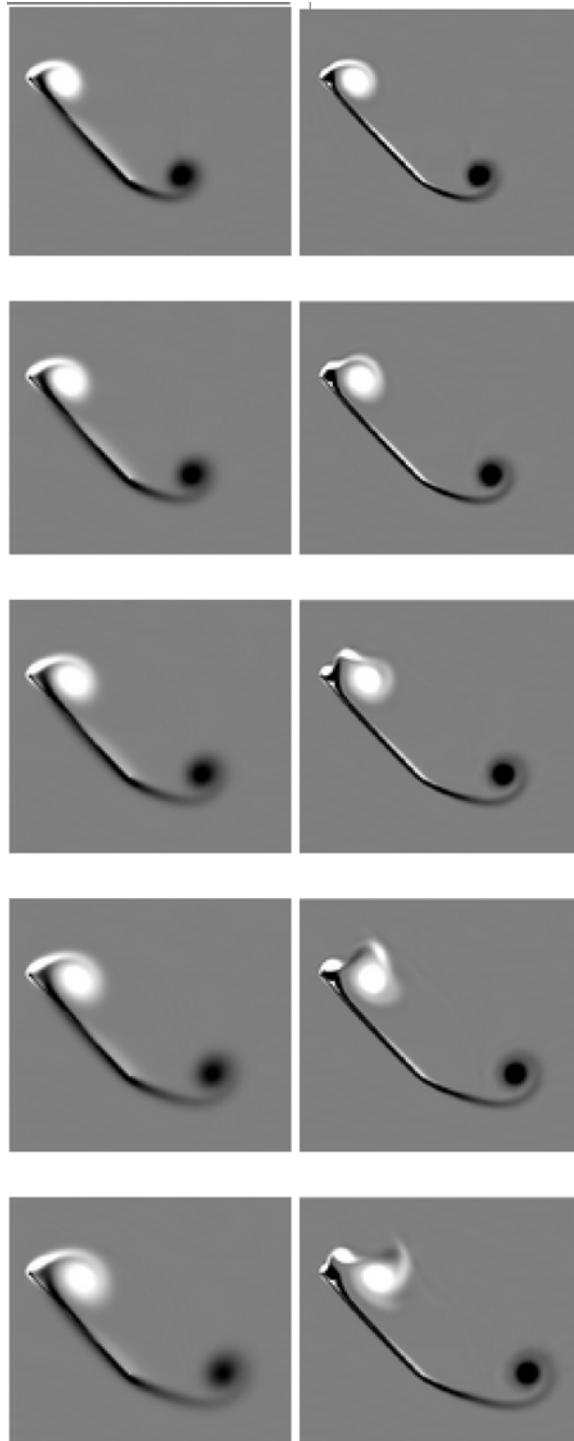
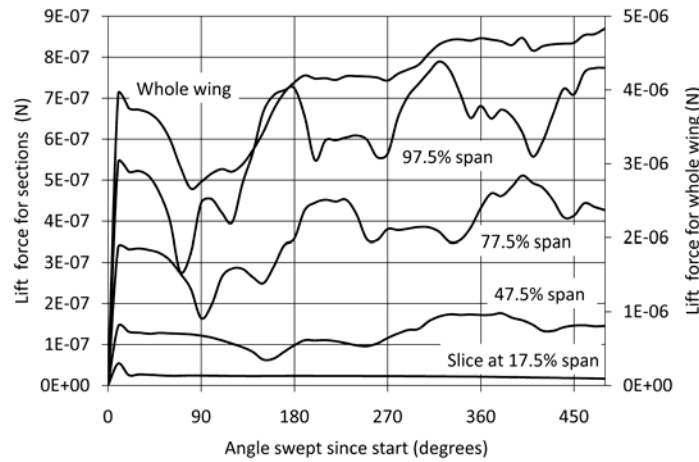


Figure 11: Contours of vorticity showing comparison of flow evolution for two Reynolds numbers;  $Re = 500$  (left-hand column) and  $Re = 5000$  (right-hand column). Light areas show clockwise vorticity, dark areas show anti-clockwise vorticity. The aerofoil has moved around 0.5 chords since being impulsively started at the start of the sequence (top of figure).



**Figure 13: Lift contribution from four wing sections, along with total wing lift, predicted using aerodynamic model. Note that the wing is made up of more sections than are shown here. Wing is rectangular planform and angle of attack is  $45^\circ$ .**

It can be seen that a streamline released from the leading edge at the wing root eventually leaves the trailing edge at around 75% span. The aerodynamic model cannot capture this spanwise flow (as it divides the wing into 2D slices and then analyses each slice individually), and will predict the leading-edge vortex continually building up and shedding as for the 2D flows above. Thus the lift produced by each section will continually fluctuate. This is shown in Figure 13, where the lift contributions from four of the slices are shown, along with the total lift for the entire wing. It can be seen that the total lift produced by the wing is relatively steady after around  $180^\circ$  of sweep rotation, even though the contributions from the component slices are unsteady. As we would expect, outboard sections contribute more lift as they are moving faster than inboard sections. The lift contribution from a section also depends on the local chord, so an elliptical-planform wing would gain little contribution from the sections close to the tip.

Figure 14 compares lift predictions for 3D wings for the aerodynamic model and the CFD model. Once again, due to the fact that the aerodynamic model is Reynolds-number independent, CFD results are given for two Reynolds numbers, though in this case the difference between the data for the two Reynolds numbers is less dramatic.

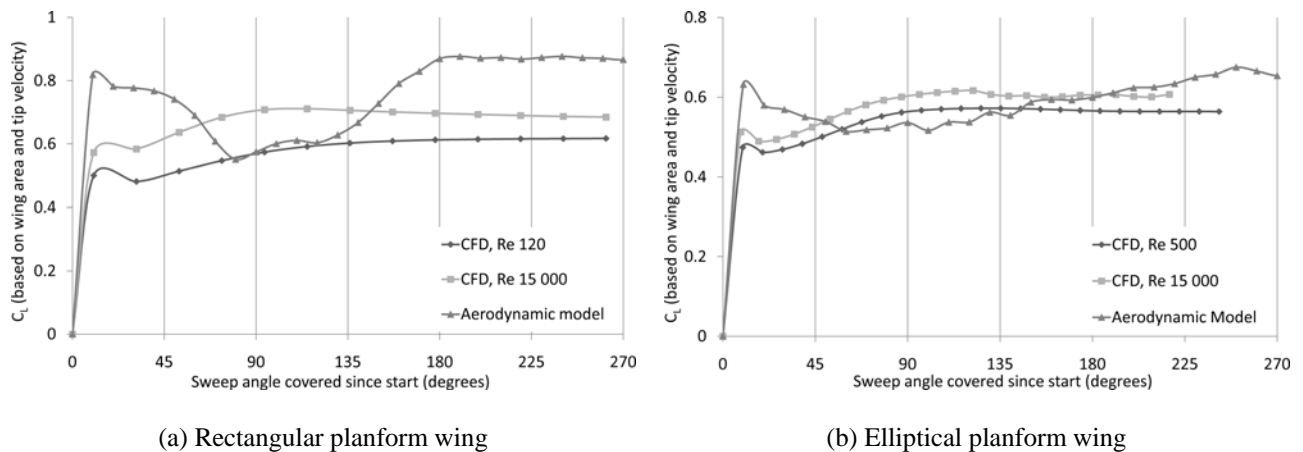


**Figure 14: Comparison of lift predictions from aerodynamic model and CFD model for two wing planforms.**

The agreement is not as good as for the 2D cases, as we might expect. However both models predict lift coefficients of the same order of magnitude and both models show an eventual stabilising of the lift. It is important to emphasise again that we are using the aerodynamic model in a case for which it was not designed – it was designed for insect-like flapping, when the wings would not sweep through such large angles.

Dickinson carried out force measurements using an artificial flapper, Robofly (see: [9]; [13]; [16]). During these tests force measurements were obtained for a flapping 3D wing. We compare these with data from the aerodynamic model in Figure 15. Remarkable agreement can be seen suggesting that the model is capturing the important flow physics.

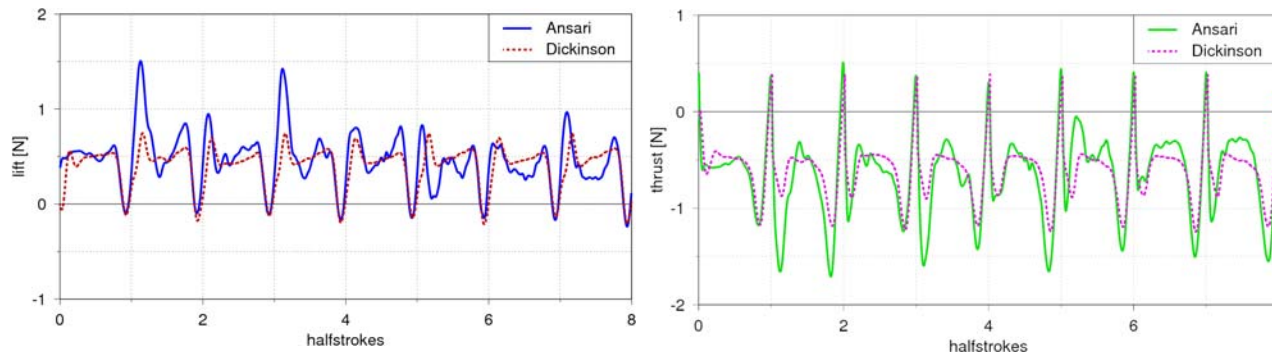


**Figure 15: Lift (left) and drag or thrust (right) force comparisons for a 3D flapping wing - Ansari's numerical predictions [16] and benchmark experiments [9].**

### Aeroelasticity

The aerodynamic model of Ansari, discussed above, has recently been used in an integrated fashion with new experimental studies to investigate wing aeroelasticity. In flight measurements were taken by our partners using photogrammetric techniques [20]. These were combined with aerodynamic data from Ansari's model and a new elastic deflection model to investigate the relative importance of aeroelastic and inertioelastic deformation. Details are provided in Knowles et al [21].

### Conclusions

Since FMAVs will operate at relatively low Reynolds numbers ( $\sim 35000$ , based on mean chord and peak tip velocity) at which viscous forces might be thought to be dominant, and since FMAV wings are known to experience three-dimensional flow effects, the accuracy of Ansari's model when compared to experimental data is surprising. This paper has investigated a number of issues related to this.

It has been shown for 2D flows that as chord Reynolds numbers increase from  $O(100)$  to  $O(10000)$  there are instabilities in the vortex sheets shed from leading and trailing edges. These give rise to higher-frequency force fluctuations than are seen in Ansari's model or in low-Reynolds number experiments.

The effect of varying wing cross-section has been examined in order to identify important features which may be needed for an 'optimum' cross-section for a successful FMAV. Little effect of cross-section has been identified.

We have shown that for 2D flows the leading-edge vortex is unstable for all but the very lowest ( $< 50$ ) Reynolds numbers. However, stable leading-edge vortices are thought to be a fundamental part of the reason for the high lift forces produced by insect wings. Our CFD results show that a rotating 3D wing at high angle of attack produces a conical leading-edge vortex, as has been seen in physical experiments. The development of this LEV depends on

Reynolds number. For lower Reynolds numbers it is stable for all time, with higher Reynolds numbers producing larger LEVs. If Reynolds number is increased above a critical value, Kelvin-Helmholtz instability occurs in the leading-edge vortex sheet, resulting in the sheet breaking down on outboard sections of the wing. However, this breakdown has little effect on the lift produced by the wing, because the LEV does not break away from the wing completely as it does for 2D flows — a von Kármán street-like structure is not seen. This is confirmed by physical experiments. The lift produced by a 3D wing is therefore more stable than that produced by a 2D aerofoil. Finally, it has also been demonstrated that a rotary wing motion is an essential element in providing a stable LEV.

Overall, the successful development of an operational flapping-wing micro air vehicle will depend on major progress in a number of technology areas. In aerodynamics, this paper has shown how an integrated approach, involving aerodynamic modelling, CFD and experimentation is leading to improved understanding of the flapping-wing problem and, hence, a wing design capability (covering aerodynamics, wing kinematics and aeroelastics).

## Acknowledgements

The authors gratefully acknowledge the support of the UK's Engineering and Physical Sciences Research Council and the Ministry of Defence Joint Grant Scheme: work presented here has been partly supported by grants GR/M78472, GR/M22970 & GR/S23025/01. The second author (PCW) has been supported during his PhD work by a bursary from the Department of Aerospace, Power and Sensors, Cranfield University.

## References

- [1] R. Zbikowski, Flapping Wing Autonomous Micro Air Vehicles: Research Programme Outline, in *14th Int. Conf. on Unmanned Air Vehicle Systems*, vol. Supplementary Papers, 1999, pp. 38.1–38.5.
- [2] R. Zbikowski, Flapping Wing Micro Air Vehicle: A Guided Platform for Microsensors, in *RAeS Conf. on Nanotechnology and Microengineering for Future Guided Weapons*, 1999, pp. 1.1–1.11.
- [3] R. Zbikowski, Flapping Wing Technology, in *European Military Rotorcraft Symposium*, Shrivenham, UK, 21–23 March 2000, pp. 1–7.
- [4] R. Dudley, *Biomechanics (Structures & Systems): A Practical Approach*, OUP, 1992.
- [5] R. Zbikowski, C B Pedersen, S A Ansari & C Galinski, Flapping Wing Micro Air Vehicles, *Lecture Series: Low Reynolds Number Aerodynamics on Aircraft Including Applications in Emerging UAV Technology*, RTO/AVT 104, von Karman Institute, Belgium, 2003.
- [6] M. I. Woods, J. F. Henderson, and G. D. Lock, Energy Requirements for the Flight of Micro Air Vehicles, *Aeronautical Journal*, **105**:135–149, 2001.
- [7] C. P. Ellington, The Aerodynamics of Hovering Insect Flight: III. Kinematics, *Philosophical Transactions of the Royal Society of London Series B*, **305**:41–78, 1984.
- [8] A. R. Ennos, The Kinematics and Aerodynamics of the Free Flight of Some Diptera, *Journal of Experimental Biology*, **142**:49–85, 1989.
- [9] M. H. Dickinson, F.-O. Lehmann & S. P. Sane, Wing Rotation and the Aerodynamic Basis of Insect Flight, *Science*, **284**:1954–1960, 1999.
- [10] R. Zbikowski, On Aerodynamic Modelling of an Insect-like Flapping Wing in Hover for Micro Air Vehicles, *Philosophical Transactions of the Royal Society of London Series A*, **360**:273–290, 2002.

- [11] C. P. Ellington, C. van den Berg, A. P. Willmott & A. L. R. Thomas, Leading-edge Vortices in Insect Flight, *Nature*, **384**:626–630, 1996.
- [12] H. Liu, C. P. Ellington, , K. Kawachi, , C. van den Berg, , & A. P. Wilmott, A Computational Fluid Dynamic Study of Hawkmoth Hovering, *Journal of Experimental Biology*, **201**:461–477, 1998.
- [13] S. A. Ansari, *A Nonlinear, Unsteady, Aerodynamic Model for Insect-like Flapping Wings in the Hover with Micro Air Vehicle Applications*, PhD thesis, Department of Aerospace, Power and Sensors, Cranfield University, Shrivenham, 2004.
- [14] S.A. Ansari, R. Zbikowski, and K. Knowles, Aerodynamic Modelling of Insect-like Flapping Flight for Micro Air Vehicles, *Progress in Aerospace Sciences*, **42** (2): 129-172, 2006.
- [15] S.A. Ansari, R. Zbikowski & K. Knowles, A Nonlinear Unsteady Aerodynamic Model for Insect-like Flapping Wings in the Hover: Part I. Methodology and Analysis, *Proceedings IMechE Part G: Journal of Aerospace Engineering*, **220** (G2):61-83, 2006.
- [16] S.A. Ansari, R. Zbikowski & K. Knowles, A Nonlinear Unsteady Aerodynamic Model for Insect-like Flapping Wings in the Hover: Part II. Implementation and Validation, *Proceedings IMechE Part G: Journal of Aerospace Engineering*, **220** (G3):169-186, 2006.
- [17] S.A. Ansari, K. Knowles & R. Zbikowski, Design Guidelines for Flapping-Wing Micro UAVs, *Int. Powered Lift Conf.*, Grapevine, TX, 3-6 October 2005. Pub: SAE Paper no 2005-01-3197.
- [18] M. H. Dickinson & K. G. Götz, Unsteady Aerodynamic Performance of Model Wings at Low Reynolds Numbers, *Journal of Experimental Biology*, **174**: 45–64, 1993.
- [19] W. Thomson (Lord Kelvin), On Vortex Motion, In *Mathematical and Physical Papers: Volume IV Hydrodynamics and General Dynamics*. Cambridge University Press, 1910.
- [20] I. Wallace, N. J. Lawson, A. R. Harvey, J. D. C. Jones, and A. J. Moore. High-speed photogrammetry system for measuring the kinematics of insect wings. *Applied Optics*, 45(17):4165–4173, 2006.
- [21] K. Knowles, S.A. Ansari, P.C. Wilkins, and R.W. Zbikowski, "Recent Progress Towards Developing an Insect-inspired Flapping-wing Micro Air Vehicle", *AVT146 "Platform Innovations and System Integration for Unmanned Air, Land and Sea Vehicles"*, Florence, Italy, 14-18 May 2007. Pub: RTO
- [22] W. Merzkirch, *Flow Visualization*, Academic Press, Inc., 1987 (2<sup>nd</sup> Edition)
- [23] P. G. Drazin & W. H. Reid, *Hydrodynamic Stability*, Cambridge University Press, 1981
- [24] P.C. Wilkins and K. Knowles, "Investigation of Aerodynamics Relevant to Flapping-wing Micro Air Vehicles", *AIAA 37th Fluid Dynamics Conference*, Miami, FL, 25 - 28 June 2007. Pub: AIAA Paper no AIAA-2007-4338.